

Regulation of actin cytoskeleton via photolithographic micropatterning

Fulin Xing*, Haimei Zhang*, Mengyu Li*, Hao Dong*, Xuehe Ma*, Shiyu Deng*,
Fen Hu*, Imshik Lee*, Leiting Pan*,†,‡,§,¶ and Jingjun Xu*,§

**The Key Laboratory of Weak-Light Nonlinear Photonics of Education Ministry
School of Physics and TEDA Institute of Applied Physics
Nankai University, Tianjin 300071 P. R. China*

†*State Key Laboratory of Medicinal Chemical Biology
Frontiers Science Center for Cell Responses
College of Life Sciences
Nankai University, Tianjin 300071, P. R. China*

‡*Collaborative Innovation Center of Extreme Optics
Shanxi University, Taiyuan Shanxi 030006, P. R. China*

§*Shenzhen Research Institute of Nankai University
Shenzhen, Guangdong 518083, P. R. China
¶plt@nankai.edu.cn*

Received 27 July 2022

Accepted 4 October 2022

Published 16 November 2022

Actin cytoskeleton plays crucial roles in various cellular functions. Extracellular matrix (ECM) can modulate cell morphology by remodeling the internal cytoskeleton. To define how geometry of ECM regulates the organization of actin cytoskeleton, we plated individual NIH 3T3 cells on micropatterned substrates with distinct shapes and sizes. It was found that the stress fibers could form along the nonadhesive edges of T-shaped pattern, but were absent from the opening edge of V-shaped pattern, indicating that the organization of actin cytoskeleton was dependent on the mechanical environment. Furthermore, a secondary actin ring was observed on 50 μm circular pattern while did not appear on 30 μm and 40 μm pattern, showing a size-dependent organization of actin cytoskeleton. Finally, osteoblasts, MDCK and A549 cells exhibited distinct organization of actin cytoskeleton on T-shaped pattern, suggesting a cell-type specificity in arrangement of actin cytoskeleton. Together, our findings brought novel insight into the organization of actin cytoskeleton on micropatterned environments.

Keywords: Actin cytoskeleton; photolithography; micropatterning; extracellular matrix.

1. Introduction

Cytoskeleton plays a crucial role in various cellular process, such as cell locomotion, cell division and intercellular transport.^{1–4} It is widely accepted that there are three main types of cytoskeletons, namely microtubules, actin filaments and intermedia filaments.^{5–7} Actin cytoskeleton, also known as F-actin, consists of G-actin that form two right-handed steep helices.^{8,9} An F-actin has a barbed, fast-growing ends pointing towards the direction of membrane protrusion and a slow end towards cytoplasma.^{10,11} As highly dynamic cytoskeleton components, actin dictates the intracellular force generation, cell adhesion, cell migration, etc.^{12–14} At the tissue level, some supracellular actin structures, e.g. purse-string structures, are essential for wound healing closure and embryonic development.^{15,16} Cells adapt to different mechanical cues, such as spatial confinement and ununiform substrates, to enable shape changes, adhesion and movement through the rearrangement of actin cytoskeleton.³ Therefore, it is of great importance to understand the organization of actin cytoskeleton in different patterns of extracellular matrix (ECM).

A great deal of techniques has been developed to manipulate single cells, such as optical tweezers,¹⁷ microfluidics¹⁸ and laser microdissection.¹⁹ The emergence of micropatterning technique provided an opportunity to precisely control the morphology of single cells in a high-throughput and relatively easy-to-use manner. Micropatterning allows standardization of the ECM and cell shape, leading to an in-depth understanding of the regulatory mechanisms of cell cytoskeleton, interaction between organelles and cell fate from the perspective of cell morphology.²⁰ On the other hand, micropatterning creates specific conditions to induce the formation of subcellular structures, such as stress fibers²¹ and podosomes,^{22,23} providing convenience for associated studies.

In this study, we applied photolithographic micropatterning to create different adhesive patterns to investigate the influence of ECM geometry on the organization of actin cytoskeleton. In addition, different cell types, including osteoblasts, MDCK and A549 cells were also tested on micro-patterned ECM.

2. Materials and Methods

2.1. Photolithographic micropatterning

We chose photolithographic micropatterning that was derived from semiconductor industry because it allows a high-resolution and mass-produced micropatterning for the cells. The micropatterned substrates were fabricated as previously described.²⁴ In brief, glass coverslips ($\varphi = 20$ mm) were cleaned thoroughly in solution containing sulfuric acid and potassium dichromate. Then, the coverslip was placed inside a vacuum drier containing hexamethyldisilane (HMDS, Sigma, USA) vapor to enable deposition of HMDS for 30 min. For photolithographic micropatterning, a positive photoresist was spun onto the coverslip evaporated with HMDS. Then, the coverslip was mounted on a mask aligner (Midas, Korea) and exposed by UV light through a cadmium-based mask. Afterwards, exposed part of the photoresist was washed by developing liquid so that underlying HMDS could be removed by an oxygen plasma. Then, the remaining photoresist was removed by acetone, isopropanol and deionized water, respectively. For surface passivation, the coverslip was treated with a poly-L-lysine grafted polyethylene glycol (pLL-PEG, Susos, Switzerland) solution in phosphate-buffered saline (PBS). For cell adhesion, the coverslip was treated with a fibronectin (FN, Biotum, USA) solution in PBS. To label the FN with fluorescent probe, the FN solution was mixed with CF488A dye (Biotum, USA). The corresponding schematic diagram was shown in Fig. 1(a).

2.2. Cell culture and adhesion

NIH 3T3, lifeact-RFP-expressing NIH 3T3, MDCK and A549 cells were cultured in Dulbecco's modified Eagle's medium (Gibco, USA) with 10% (v/v) fetal bovine serum, 100 U/mL penicillin, and 100 μ g/mL streptomycin (Gibco, USA) under the condition of 37°C and 5% CO₂. Before experiments, the cells were detached with trypsin (Gibco, USA) and adjusted to the density of $6\text{--}8 \times 10^5$ mL⁻¹. Then the cell suspension was added onto the coverslip and incubated in 37°C and 5% CO₂ for adhesion. Afterwards, the coverslip was washed gently to remove suspended cells for further experiments. Adhered cells were incubated for ~4 h to allow cell

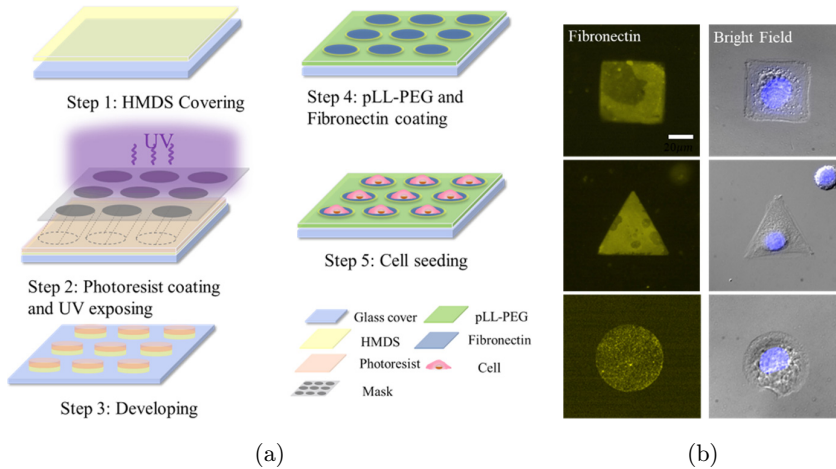


Fig. 1. Fabrication of micropatterns. (a) Schematic diagram of substrate preparation based on photolithographic micropatterning. (b) NIH 3T3 cells cultured on square, triangular and circle patterns. Left column are fluorescent images of patterned FN. Right column are bright field images of corresponding cells. Scale bar, 20 μ m.

spreading. The mouse osteoblasts were isolated and cultured as previously described.²⁵ Micropatterning for osteoblasts, MDCK and A549 cells followed the same steps. The shapes of the cells were controlled precisely according to the pattern [Fig. 1(b)].

2.3. Immunofluorescence

The sample was fixed by 4% (w/v) paraformaldehyde in PBS for 20 min. Then the cells were permeabilized and blocked in a blocking buffer (3% w/v BSA, 0.5% v/v Triton X-100 in PBS) for 20 min. After that, the cells were incubated with $\sim 0.4 \mu$ M Alexa647-phalloidin ((Invitrogen, USA) in the blocking buffer for 1 h at room temperature. After washing in PBS for three times, the samples were ready for imaging.

The images of cells labeled with Alexa647-phalloidin were obtained by an invert microscopy (Olympus, Japan) mounted with a CCD camera (Regita R1, Qimaging, Canada). The cells were excited by a mercury lamp using a 647 nm excitation filter, and fluorescence emission was collected by a 40 \times /1.30 oil objective. The obtained images were aligned by imageJ equipped with StackReg plugin. This plugin first designated a certain image in the experimental data as a reference and automatically extracted image features. Afterwards, displacement transformation on other images was carried out. Finally, a series of image data were automatically aligned, so as to reveal the special structural characteristics of the cytoskeleton under the restriction of single cell pattern. The following

averaging of images was performed by a custom MATLAB program.

2.4. Data analysis

Data are presented as mean \pm standard error of mean (SEM). Comparison between the two groups was performed using unpaired Student's *t* test (GraphPad Prism). Statistical significance was defined as **P* < 0.05, ***P* < 0.01, ****P* < 0.001, n.s., no significance.

3. Results and Discussions

3.1. Geometry of ECM pattern regulated the arrangement of actin cytoskeleton

To test how ECM geometry regulates the organization of actin cytoskeleton, we designed several triangular-derived patterns with a 50 μ m side length, including normal triangular pattern, V-shaped pattern and T-shaped pattern [Fig. 2(a)]. Cells plated on these patterns exhibited a similar triangular morphology. Notably, cells formed curved outlines along the nonadhesive upper edges in the V-like pattern and along the nonadhesive bilateral edges in the T-like pattern. The organization of actin cytoskeleton was also distinctive among these patterns [Fig. 2(b)]. In detail, actin assembled as stress fibers along the three sides of the triangular pattern with a relative high fluorescence intensity compared to that of the interior of the cell. However, in the V-shaped pattern,

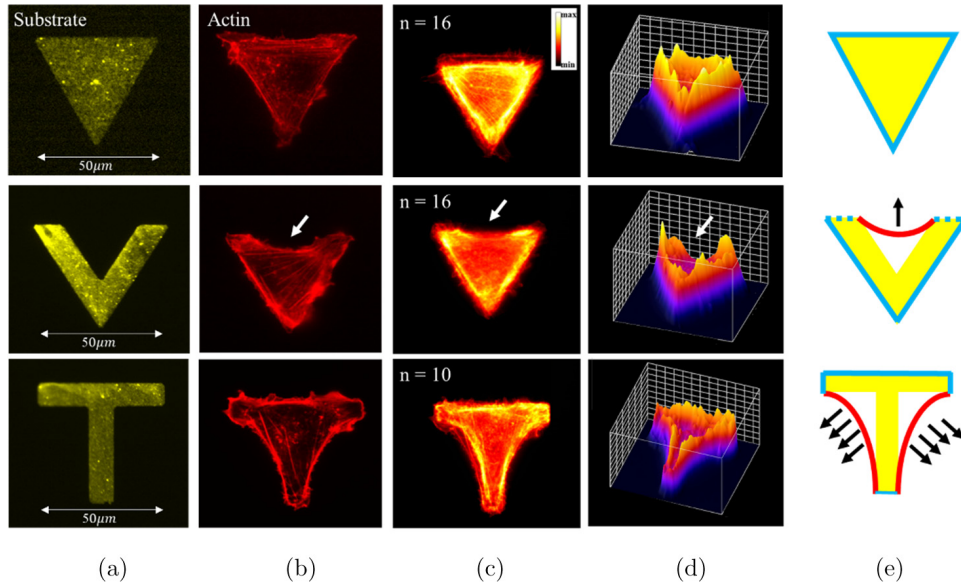


Fig. 2. The organization of actin cytoskeleton in NIH 3T3 cells on triangular-derived patterns. (a) Fluorescent images of patterned FN of triangular pattern, V-shaped pattern and T-shaped pattern. (b) Representative images of individual NIH 3T3 cells labeled by Alexa647-phalloidin on three patterns. (c) Averaged imaged of actin on three patterns. Data was derived from 16, 16 and 10 cells, respectively. (d) 3D plot of images in C. (e) Schematic showing the mechanism of stress fiber formation on three patterns (yellow). Briefly, cells form stress fibers along adhesive edges (blue) on triangular pattern. On V-shaped pattern, adhesive edges (dashed blue) extend into the nonadhesive edge (red) from two directions, sharing the tension along this side. On T-shaped pattern, the tension along the nonadhesive edge needs the stress fiber to maintain the morphology of the cell.

the stress fiber was absent from the opening nonadhesive edge of the pattern. On the contrary, cells on the T-shaped pattern formed enriched stress fiber along both nonadhesive edges of the pattern. The averaged result obtained from more than 10 cells and their 3D plots confirmed that the actin did not assemble on the opening of V-shaped pattern while formed stress fiber along the nonadhesive edge of T-shaped pattern [Figs. 2(c) and 2(d)]. Actin stress fibers could provide contractile forces that maintained cell morphology in different mechanical environments.^{26,27} In T-shaped patterns, stress fibers were formed along the nonadhesive edges to maintain the triangular-like shape. But in the V-shaped pattern, two adhesive edges extended into the nonadhesive edges from both sides [Fig. 2(e)], which may share tension of the cell edge. In this case, stress fibers were no longer needed to provide the tension.

We then quantitatively compared the relative fluorescence intensity of the stress fiber between different patterns, which was shown by the ratios of the average fluorescence intensity along the edge divided by the average intensity inside the cell (Fig. 3). The results showed that the ratio of the three edges in the triangular pattern was approximately the same (1.65 ± 0.10 , 1.59 ± 0.13 and 1.74 ± 0.13 for left,

right and upper edge, Fig. 3(a)). On the contrary, in the V-like pattern, the ratio of the upper opening edge (1.17 ± 0.02) was smaller than those of the adhesive edge (left edge, 1.33 ± 0.04 , right edge, 1.32 ± 0.02) [Fig. 3(b)]. In T-shaped pattern, the ratios along the three edges showed no significance (1.39 ± 0.11 , 1.27 ± 0.06 and 1.46 ± 0.10 for left, right and upper edges) [Fig. 3(c)]. These results indicated that the cells need to form stress fibers to maintain the morphology rather than spreading lamellipodia. The contractile mechanical environment will lead to curved edges along the nonadhesive sides.

Furthermore, we designed a triadius pattern and a slender V-like pattern (Fig. S1). The opening angle of the upper edge in the triadius pattern was larger than that in the slender V pattern. It was found that the stress fiber formed along the upper opening edge in both patterns [Figs. S1(A) and S1(B)] while the intensity of the stress fiber in the triadius pattern (ratio = 1.67 ± 0.08) was higher than that in the slender V pattern (ratio = 1.33 ± 0.06), suggesting that cells need more intensive stress fiber to maintain the morphology along edges with larger opening angles. Together, these results demonstrated that the organization of actin cytoskeleton depended on the

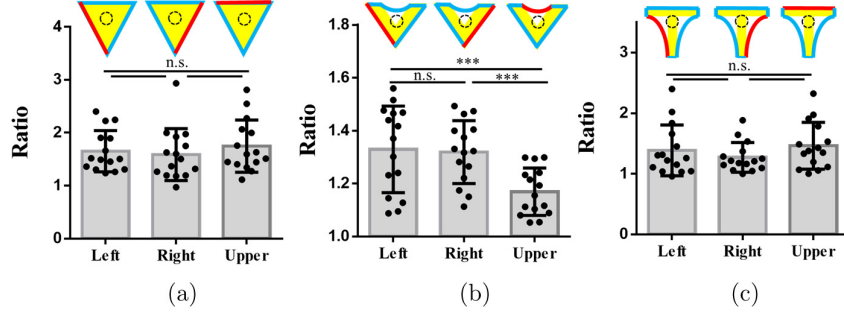


Fig. 3. The statistical data of the ratio in the triangular pattern (a), V-like pattern (b) and the T-like pattern (c). The ratios were obtained from the averaged intensity along the edges (red edges) divided by the average intensity in the circular region in the cell (dashed black circles). Student's *t* test, ***, $P < 0.001$. N.s., no significance.

mechanical environment, rather than the envelopes of ECM geometry.

3.2. Size of ECM pattern regulated the organization of actin cytoskeleton

To determine the effect of pattern size on the organization of actin cytoskeleton, we used circular

patterns with different diameters of 30, 40 and 50 μm , respectively [Fig. 4(a)]. Cells on 30 μm and 40 μm pattern formed stress fiber along the circumference. Interestingly, on the 50 μm pattern, a secondary actin ring was observed inside the circle [Figs. 4(b) and 4(c)]. Further 3D plots clearly showed the secondary ring of actin [Fig. 4(d)].

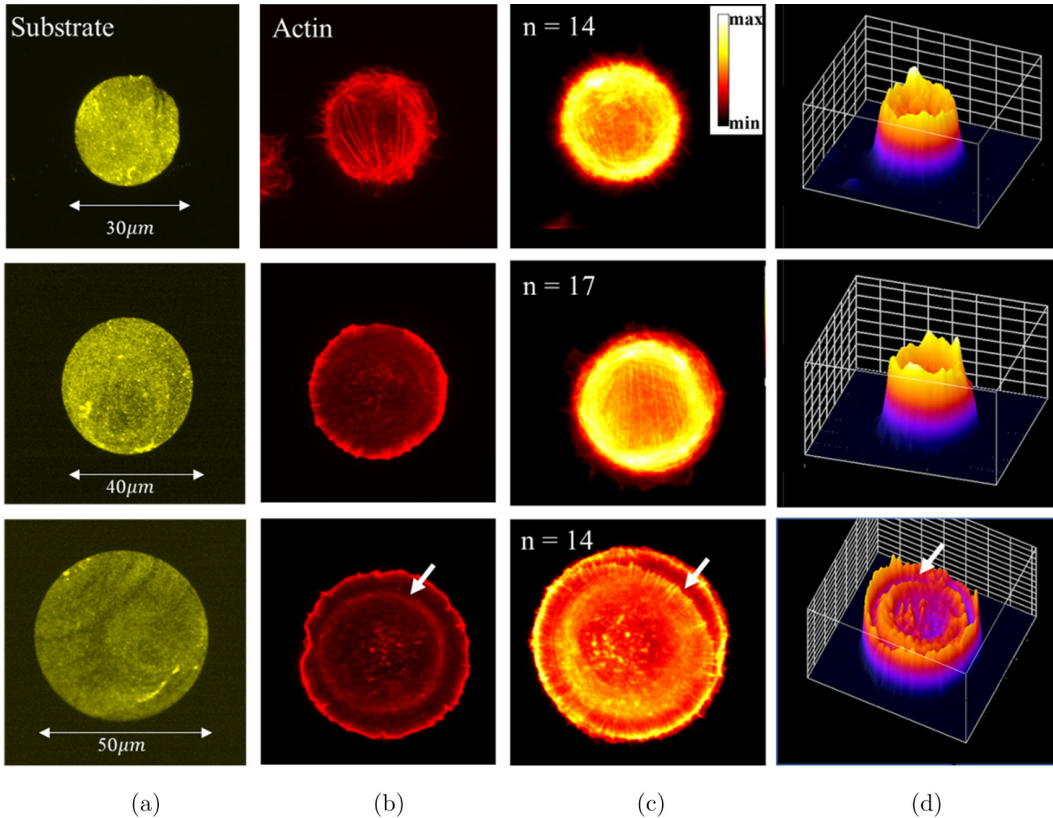


Fig. 4. The organization of actin cytoskeleton in NIH 3T3 cells on circular patterns with different diameters. (a) FN micropatterns of circular patterns with diameter of 30, 40 and 50 μm . (b) Representative images of individual NIH 3T3 cells labeled with Alexa647-phalloidin on three circular patterns. A secondary ring of actin was observed on 50 μm pattern (white arrow). (c) Averaged images of actin on three patterns. Data was derived from 14, 17 and 14 cells, respectively. The secondary ring of actin was indicated by the white arrow. (d) 3D plot of images in C. A clear secondary ring of actin was shown on 50 μm pattern (white arrow).

These results demonstrated that the organization of actin cytoskeleton was dependent on the size of the pattern. For all patterns, cells needed stress fibers along the circumference to keep spreading and maintain the cell shape. We also designed the square pattern and the shuriken-like pattern to confine the NIH 3T3 cells. Interestingly, the second ring exhibited a square appearance in the square pattern, while a circular ring in the shuriken-like pattern [Fig. S2(A)]. Although cells displayed a square-like morphology in both patterns, the shape of secondary actin ring was distinct, illustrating that the underlying mechanical environments could modulate the organization of cytoskeleton.

With respect to the secondary actin ring, we reasoned that on the pattern of $50\text{ }\mu\text{m}$ diameter, the formation of secondary actin ring may be associated with the retrograde flow of actin. Actin polymerization at the leading edge drives the membrane protrusion, while retrograde flow governs the movement of actin network away from the leading

edge.^{28,29} The balance of actin polymerization and retrograde flow dictates the cell motion and cell shapes.³⁰ In the circular pattern, the actin polymerized and formed stress fibers along the circumference while actin retrograde flow balanced the spreading of the cell. On the other hand, it was easy to imagine that when the cell spreads to a larger area (e.g. $50\text{ }\mu\text{m}$ pattern), the nucleus and other cellular components would be squashed on the substrates, resulting in a barrier that blocked actin retrograde flow at the position of rings. To verify the hypothesis, we used NIH 3T3 cells transfected with lifeact-RFP to observe the retrograde flow of actin cytoskeleton. The time-lapse imaging exhibited a retrograde flow along the periphery that was cut off around the interior of the circular pattern (Figs. S2(B) and S2(C), Movie S1). Furthermore, the DIC image showed that the ring is located around the nucleus and other cellular components [Fig. S2(D)]. These secondary actin rings in turn may provide a mechanical support for the nucleus.³¹

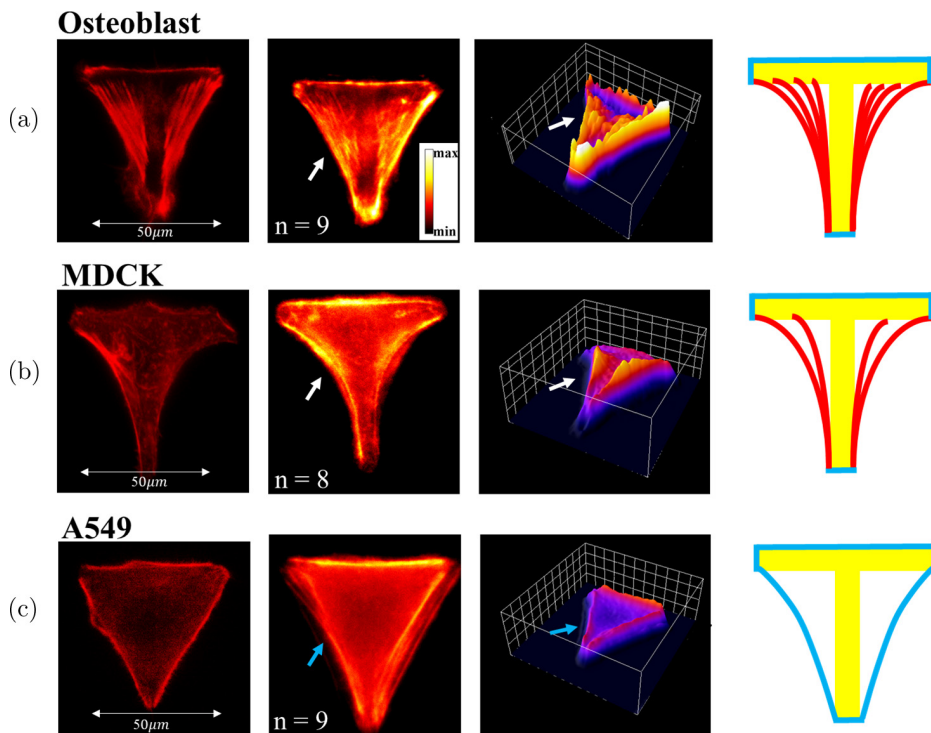


Fig. 5. Organization of actin cytoskeleton in osteoblast (a), MDCK (b) and A549 cells (c) on T-shaped patterns. Stress fibers formed along the nonadhesive edges in osteoblasts and MDCK cells (white arrow), but was absent in A549 cells (blue arrow). First column, representative images of cells labeled with F-actin. Second column, averaged image of actin in three types of cells. Third column, 3D plots of images in the second column. Fourth column, schematic showing the stress fiber formation (red) of three types of cells.

3.3. Different cell types exhibited distinct organization of actin cytoskeleton

To test whether different cell types display distinct organization of actin cytoskeleton, we plated mouse osteoblasts, A549 cells (a nonsmall cell lung cancer cells) and MDCK cells (Madin–Daby canine kidney cells) on T-shaped patterns with side length of 50 μm . As shown in Fig. 5(a), osteoblasts and MDCK cells formed stress fibers along the nonadhesive edges of the T-shaped pattern. The averaged images and 3D construction confirmed that along both edges of the T-like shape, stress fibers could be observed in osteoblasts and MDCK cells, but were lack in A549 cells [Figs. 5(b) and 5(c)]. Thus, we reasoned that there were distinct cellular mechanics among different cell types, leading to a different organization of actin skeleton in the same micro-pattern. Osteoblasts assemble enriched actin stress fibers and other structures in response to complex mechanical environments.^{32,33} Similarly, MDCK cells, a model cell for cell migration research, are epithelioid cells that have enriched stress fibers.³⁴ By contrast, A549 cell showed relatively low abundance in stress fiber before the epithelial-mesenchymal transition.^{35,36} Therefore, few stress fibers were needed along the nonadhesive edges for A549 cells. Besides, there were no significant differences in the sizes of the three cell types (Fig. S3). Thus, it could be ruled out that the difference of actin organization in three types of cells is a result of different sizes of the cell. Together, our results demonstrated that different cell types can exhibit distinct organization of actin cytoskeleton in the same mechanical environments.

4. Conclusions

In this work, we mainly applied photolithographic micropatterning to regulate the actin cytoskeleton in NIH 3T3 fibroblasts. The stress fibers were assembled along the nonadhesive edges. When adhesive edges extended into nonadhesive edges, the stress fibers along on nonadhesive part disappeared, suggesting that the actin organization was regulated by the mechanical environments. A size-dependent phenomenon of actin organization that a secondary actin ring formed on large circular pattern was also found. Finally, osteoblasts and MDCK

cells exhibited stress fibers along nonadhesive edges of T-shaped pattern while stress fibers were absent for A549 cells, indicating a cell type-dependent organization of actin cytoskeleton. Our study provided further understanding of the mechanism of how ECM regulated actin cytoskeleton.

Conflicts of Interest

The authors declare that there are no conflicts of interest relevant to this article.

Acknowledgments

This work was supported by the Guangdong Major Project of Basic and Applied Basic Research (2020B0301030009), the National Key Research and Development Program of China (2022YFC3400600) National Natural Science Foundation of China (12174208, 32227802, 11874231, 31801134 and 31870843), Tianjin Natural Science Foundation (20JCYBJC01010), China Postdoctoral Science Foundation (2020M680032) and Fundamental Research Funds for the Central Universities (2122021337 and 2122021405).

References

1. A. Datta, S. Deng, V. Gopal *et al.*, “Cytoskeletal dynamics in epithelial-mesenchymal transition: Insights into therapeutic targets for cancer metastasis,” *Cancers* **13**, 1882 (2021).
2. I. Monastyrskaya, E. Rieter, D. J. Klionsky *et al.*, “Multiple roles of the cytoskeleton in autophagy,” *Biol. Rev.* **84**, 431–448 (2009).
3. T. Hohmann, F. Dehghani. “The cytoskeleton — a complex interacting meshwork,” *Cells* **8**, 362 (2019).
4. M. Shah, L. A. Chacko, J. P. Joseph *et al.*, “Mitochondrial dynamics, positioning and function mediated by cytoskeletal interactions,” *Cell. Mol. Life Sci.* **78**, 3969–3986 (2021).
5. D. D. Tang, B. D. Gerlach, “The roles and regulation of the actin cytoskeleton, intermediate filaments and microtubules in smooth muscle cell migration,” *Resp. Res.* **18**, 1–12 (2017).
6. M. Schoumacher, R. D. Goldman, D. Louvard *et al.*, “Actin, microtubules, and vimentin intermediate filaments cooperate for elongation of invadopodia,” *J. Cell Biol.* **189**, 541–556 (2010).
7. M. Dogterom, G. H. Koenderink, “Actin–microtubule crosstalk in cell biology,” *Nat. Rev. Mol. Cell Biol.* **20**, 38–54 (2019).

8. K. C. Holmes, D. Popp, W. Gebhard *et al.*, “Atomic model of the actin filament,” *Nature* **347**, 44–49 (1990).
9. R. Dominguez, K. C. Holmes, “Actin structure and function,” *Annu. Rev. Biophys.* **40**, 169 (2011).
10. R. D. Welch Mullins, “Cellular control of actin nucleation,” *Annu. Rev. Cell Dev. Biol.* **18**, 247–288 (2002).
11. M. Innocenti, “New insights into the formation and the function of lamellipodia and ruffles in mesenchymal cell migration,” *Cell Adhes. Migr.* **12**, 401–416 (2018).
12. S. H. Lee, R. Dominguez, “Regulation of actin cytoskeleton dynamics in cells,” *Mol. Cells* **29**, 311–325 (2010).
13. A. J. Davidson, W. Wood, “Unravelling the actin cytoskeleton: A new competitive edge?” *Trends Cell Biol.* **26**, 569–576 (2016).
14. A. Konietzny, J. Bär, M. Mikhaylova, “Dendritic actin cytoskeleton: Structure, functions, and regulations,” *Front. Cell. Neurosci.* **11**, 147 (2017).
15. K. E. Rothenberg, R. Fernandez-Gonzalez, “Forceful closure: Cytoskeletal networks in embryonic wound repair,” *Mol. Biol. Cell* **30**, 1353–1358 (2019).
16. S. R. K. Vedula, G. Peyret, I. Cheddadi *et al.*, “Mechanics of epithelial closure over non-adherent environments,” *Nat. Commun.* **6**, 1–10 (2015).
17. A. A. Kapkov, A. N. Semenov, P. B. Ermolinskiy *et al.*, “Forces of RBC interaction with single endothelial cells in stationary conditions: Measurements with laser tweezers,” *J. Innov. Opt. Heal. Sci.* **14**, 2142005 (2021).
18. T. Luo, L. Fan, R. Zhu *et al.*, “Microfluidic single-cell manipulation and analysis: Methods and applications,” *Micromachines* **10**, 104 (2019).
19. E. S. Park, J. P. Yan, R. A. Ang *et al.*, “Isolation and genome sequencing of individual circulating tumor cells using hydrogel encapsulation and laser capture microdissection,” *Lab Chip* **18**, 1736–1749 (2018).
20. M. Théry, V. Racine, M. Piel *et al.*, “Anisotropy of cell adhesive microenvironment governs cell internal organization and orientation of polarity,” *Proc. Natl. Acad. Sci. USA* **103**, 19771–19776 (2006).
21. E. Kassianidou, D. Probst, J. Jäger *et al.*, “Extracellular matrix geometry and initial adhesive position determine stress fiber network organization during cell spreading,” *Cell Rep.* **27**, 1897–1909. e49 (2019).
22. A. Labernadie, C. Thibault, C. Vieu *et al.*, “Dynamics of podosome stiffness revealed by atomic force microscopy,” *Proc. Natl. Acad. Sci. USA* **107**, 21016–21021 (2010).
23. N. B. M. Rafiq, Y. Nishimura, S. V. Plotnikov *et al.*, “A mechano-signalling network linking microtubules, myosin II A filaments and integrin-based adhesions,” *Nat. Mater.* **18**, 638–649 (2019).
24. F. Xing, P. Zhang, P. Jiang *et al.*, “Spatiotemporal characteristics of intercellular calcium wave communication in micropatterned assemblies of single cells,” *ACS Appl. Mater. Interfaces* **10**, 2937–2945 (2018).
25. F. Hu, Y. Zhao, Z. Hui *et al.*, “Regulation of intracellular Ca²⁺/CaMKII signaling by TRPV4 membrane translocation during osteoblastic differentiation,” *Biophys. Rep.* **5**, 254–263 (2019).
26. E. L. Elson, G. M. Genin, “The role of mechanics in actin stress fiber kinetics,” *Exp. Cell Res.* **319**, 2490–2500 (2013).
27. S. Tojkander, G. Gateva, P. Lappalainen, “Actin stress fibers—assembly, dynamics and biological roles,” *J. Cell Sci.* **125**, 1855–1864 (2012).
28. K. Wilson, A. Lewalle, M. Fritzschke *et al.*, “Mechanisms of leading edge protrusion in interstitial migration,” *Nat. Commun.* **4**, 1–12 (2013).
29. G. L. Ryan, N. Watanabe, D. Vavylonis, “A review of models of fluctuating protrusion and retraction patterns at the leading edge of motile cells,” *Cytoskeleton* **69**, 195–206 (2012).
30. J. Zimmermann, C. Brunner, M. Enculescu *et al.*, “Actin filament elasticity and retrograde flow shape the force-velocity relation of motile cells,” *Biophys. J.* **102**, 287–295 (2012).
31. H. Y. G. Lim, N. Plachta, “Cytoskeletal control of early mammalian development,” *Nat. Rev. Mol. Cell Biol.* **22**, 548–562 (2021).
32. A. Matsugaki, G. Aramoto, T. Nakano, “The alignment of MC3T3-E1 osteoblasts on steps of slip traces introduced by dislocation motion,” *Biomaterials* **33**, 7327–7335 (2012).
33. Z. Yang, S. Tan, Y. Shen *et al.*, “Inhibition of FSS-induced actin cytoskeleton reorganization by silencing LIMK2 gene increases the mechanosensitivity of primary osteoblasts,” *Bone* **74**, 182–190 (2015).
34. A. Saraswathibhatla, J. Notbohm, “Tractions and stress fibers control cell shape and rearrangements in collective cell migration,” *Phys. Rev. X* **10**, 011016 (2020).
35. M. J. Chen, X. J. Gao, L. N. Xu *et al.*, “Ezrin is required for epithelial-mesenchymal transition induced by TGF- β 1 in A549 cells,” *Int. J. Oncol.* **45**, 1515–1522 (2014).
36. K. Fujiki, H. Inamura, T. Miyayama *et al.*, “Involvement of Notch1 signaling in malignant progression of A549 cells subjected to prolonged cadmium exposure,” *J. Biol. Chem.* **292**, 7942–7953 (2017).